RESEARCH ARTICLE SUMMARY

PLANT SCIENCE

# The genetic and epigenetic landscape of the *Arabidopsis* centromeres

**Matthew Naish†, Michael Alonge†, Piotr Wlodzimierz†, Andrew J. Tock, Bradley W. Abramson, Anna Schmücker, Terezie Mandáková, Bhagyshree Jamge, Christophe Lambing, Pallas Kuo, Natasha Yelina, Nolan Hartwick, Kelly Colt, Lisa M. Smith, Jurriaan Ton, Tetsuji Kakutani, Robert A. Martienssen, Korbinian Schneeberger, Martin A. Lysak, Frédéric Berger, Alexandros Bousios, Todd P. Michael, Michael C. Schatz*, Ian R. Henderson***

**INTRODUCTION:** The centromeres of eukaryotic chromosomes assemble the multiprotein kinetochore complex and thereby position attachment to the spindle microtubules, allowing chromosome segregation during cell division. The key function of the centromere is to load nucleosomes containing the CENTROMERE SPECIFIC HISTONE H3 (CENH3) histone variant [also known as centromere protein A (CENPA)], which directs kinetochore formation. Despite their conserved function during chromosome segregation, centromeres show radically diverse organization between species at the sequence level, ranging from single nucleosomes to megabase-scale satellite repeat arrays, which is termed the centromere paradox. Centromeric satellite repeats are variable in sequence composition and length when compared between species and show a high capacity for evolutionary change, both at the levels of primary sequence and array position along the chromosome. However, the genetic and epigenetic features that contribute to centromere function and evolution are incompletely understood, in part because of the challenges of centromere sequence assembly and functional genomics of highly repetitive sequences. New long-read DNA sequencing technologies can now resolve these complex repeat arrays, revealing insights into centromere architecture and chromatin organization.

**RATIONALE:** *Arabidopsis thaliana* is a model plant species; its genome was first sequenced in 2000, yet the centromeres, telomeres, and ribosomal DNA repeats have remained unassembled, owing to their high repetition and similarity. Genomic repeats are difficult to assemble from fragmented sequencing reads, with longer, high-identity repeats being the most challenging to correctly assemble. As sequencing reads have become longer and more accurate, eukaryotic de novo genome assemblies have captured an increasingly complete picture of the repetitive component of the genome, including the centromeres. For example, Oxford Nanopore Technologies (ONT) reads have become longer and more accurate, now reaching >100 kilo–base pairs (kbp) in length with 95 to 99% modal accuracy. PacBio high-fidelity (HiFi) reads, although shorter (~15 kbp), are >99% accurate. Using ONT and HiFi reads, it is possible to bridge across interspersed unique marker sequences and accurately assemble centromere sequences. In this study, we used long-read DNA sequencing to generate a genome assembly of the *A. thaliana* accession Columbia (Col-CEN) that resolves all five centromeres. We use the Col-CEN assembly to derive insights into the chromatin and recombination landscapes within the *Arabidopsis* centromeres and how these regions evolve.

**RESULTS:** The Col-CEN assembly reveals that the *Arabidopsis* centromeres consist of megabase-scale tandemly repeated satellite arrays, which support high CENH3 (the centromere-specific histone variant that recruits kinetochores) occupancy and are densely DNA methylated. We show patterns of higher-order repetition within centromeres and that many satellite variants are private to each chromosome, which has implications for the recombination pathways acting in the centromeres. CENH3 preferentially occupies the satellites with the least amount of divergence and that show higher-order repetition. The *Arabidopsis* centromeres are mainly composed of satellite repeats that are ~178 bp in length, termed the *CEN180* satellites. *Arabidopsis* centromeres have also been invaded by *ATHILA* long terminal repeat–class retrotransposons, which disrupt the genetic and epigenetic organization of the centromeres. Using chromatin immunoprecipitation sequencing (ChIP-seq) and immunofluorescence, we demonstrate that the centromeres show a hybrid chromatin state that is distinct from euchromatin and heterochromatin. We show that crossover recombination is suppressed within the centromeres, yet low levels of meiotic double-strand breaks occur, which are regulated by DNA methylation. Together, our Col-CEN assembly reveals the genetic and epigenetic landscapes within the *Arabidopsis* centromeres.

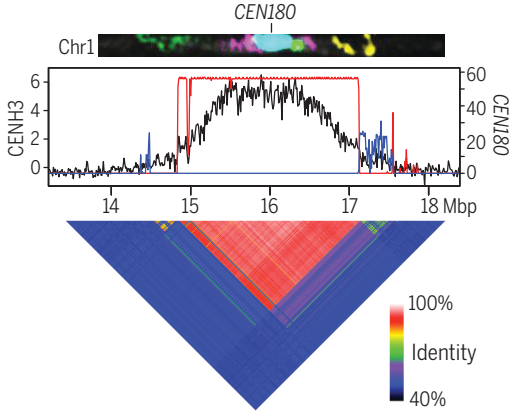


**Assembly of the *Arabidopsis* centromeres.** The structure of *Arabidopsis* centromere 1 is shown by fluorescence in situ hybridization (top) [upper-arm bacterial artificial chromosomes (BACs) (green), *ATHILA* (purple), *CEN180* (blue), the telomeric repeat (green), and bottom-arm BACs (yellow)] and a long-read genome assembly (middle). The density of centromeric histone CENH3 binding measured by ChIP-seq is shown (black), alongside the frequency of *CEN180* centromere satellite repeats. Red and blue represent forward- and reverse-strand satellites, respectively. The heatmap (bottom) shows patterns of sequence identity across the centromere between nonoverlapping 5-kbp windows. Chr, chromosome 1.

**CONCLUSION:** Our Col-CEN assembly and functional genomics analysis have implications for understanding centromere sequence evolution in eukaryotes. We propose that a recombination-based homogenization process, occurring between allelic or nonallelic locations on the same chromosome, maintains the *CEN180* library close to the consensus optimal for CENH3 recruitment. The advantage conferred to *ATHILA* retrotransposons by integration within the centromeres is presently unclear. They may be engaged in centromere drive, supporting the hypothesis that centromere satellite homogenization acts as a mechanism to purge driving elements. Each *Arabidopsis* centromere appears to represent different stages in cycles of satellite homogenization and *ATHILA*-driven diversification. These opposing forces provide both a capacity for homeostasis and a capacity for change during centromere evolution. In the future, assembly of centromeres from multiple *Arabidopsis* accessions and closely related species may further clarify how centromeres form and the evolutionary dynamics of *CEN180* and *ATHILA* repeats. ■

The list of author affiliations is available in the full article online.
***Corresponding author. Email: mschatz@cs.jhu.edu (M.C.S.); irh25@cam.ac.uk (I.R.H.)**
†These authors contributed equally to this work.
**Cite this article as M. Naish *et al.*, *Science* 374, eabi7489 (2021). DOI: 10.1126/science.abi7489**

READ THE FULL ARTICLE AT
https://doi.org/10.1126/science.abi7489

RESEARCH ARTICLE

PLANT SCIENCE

# The genetic and epigenetic landscape of the *Arabidopsis* centromeres

Matthew Naish[1]†, Michael Alonge[2]†, Piotr Wlodzimierz[1]†, Andrew J. Tock[1], Bradley W. Abramson[3], Anna Schmücker[4], Terezie Mandáková[5], Bhagyshree Jamge[4], Christophe Lambing[1], Pallas Kuo[1], Natasha Yelina[1], Nolan Hartwick[3], Kelly Colt[3], Lisa M. Smith[6], Jurriaan Ton[6], Tetsuji Kakutani[7], Robert A. Martienssen[8], Korbinian Schneeberger[9,10], Martin A. Lysak[5], Frédéric Berger[4], Alexandros Bousios[11], Todd P. Michael[3], Michael C. Schatz[2]*, Ian R. Henderson[1]*

Centromeres attach chromosomes to spindle microtubules during cell division and, despite this conserved role, show paradoxically rapid evolution and are typified by complex repeats. We used long-read sequencing to generate the Col-CEN *Arabidopsis thaliana* genome assembly that resolves all five centromeres. The centromeres consist of megabase-scale tandemly repeated satellite arrays, which support CENTROMERE SPECIFIC HISTONE H3 (CENH3) occupancy and are densely DNA methylated, with satellite variants private to each chromosome. CENH3 preferentially occupies satellites that show the least amount of divergence and occur in higher-order repeats. The centromeres are invaded by *ATHILA* retrotransposons, which disrupt genetic and epigenetic organization. Centromeric crossover recombination is suppressed, yet low levels of meiotic DNA double-strand breaks occur that are regulated by DNA methylation. We propose that *Arabidopsis* centromeres are evolving through cycles of satellite homogenization and retrotransposon-driven diversification.

Despite their conserved function during chromosome segregation, centromeres show diverse organization between species, ranging from single nucleosomes to megabase-scale tandem repeat arrays (*1*). Centromere "satellite" repeat monomers are commonly ~100 to 200 base pairs (bp) long, with each repeat capable of hosting a CENTROMERE SPECIFIC HISTONE H3 (CENH3) [also known as centromere protein A (CENPA)] variant nucleosome (*1*, *2*). CENH3 nucleosomes ultimately assemble the kinetochore and position spindle attachment on the chromosome, allowing segregation during cell division (*3*). Satellites are highly variable in sequence composition and length when compared between species (*2*). The library of centromere repeats present within a genome often shows concerted evolution, yet they have the capacity to change rapidly in structure and sequence within and between species (*1*, *2*, *4*). However, the genetic and epigenetic features that contribute to centromere evolution are incompletely understood, in large part because of the challenges of centromere sequence assembly and functional genomics of highly repetitive sequences.

Genomic repeats, especially long or high-similarity repeats, are notoriously difficult to assemble from fragmented sequencing reads (*5*). As sequencing reads have become longer and more accurate, eukaryotic de novo genome assemblies have captured an increasingly complete picture of repetitive elements. Oxford Nanopore Technologies (ONT) long reads have become substantially longer and more accurate (>100 kbp with 95 to 99% modal accuracy), owing to improved DNA extraction and library preparation, together with advanced machine learning–based base calling. Additionally, PacBio high-fidelity (HiFi) reads, although shorter (~15 kbp), are highly accurate (>99%). Using these technologies with new computational methods, researchers have assembled a complete telomere-to-telomere representation of a human genome, including the centromere satellite arrays (*6*–*8*). This work revealed that ONT and HiFi reads are sufficient to span interspersed unique marker sequences in human centromeres and other complex repeats, suggesting that truly complete genome assemblies for diverse eukaryotes are on the horizon.

*Arabidopsis thaliana* is a major model plant species; its genome was sequenced in 2000, yet the centromeres, telomeres, and ribosomal DNA repeats have remained unassembled, owing to their high repetition and similarity (*9*). The *Arabidopsis* centromeres contain millions of base pairs of the *CEN180* satellite, which support CENH3 loading (*10*–*14*). We used long-read ONT sequencing, followed by polishing with high-accuracy PacBio HiFi reads, to establish the Col-CEN reference assembly, which wholly resolves all five *Arabidopsis* centromeres from the Columbia (Col-0) accession. The assembly contains a library of 66,131 *CEN180* satellites, with each chromosome possessing mostly private satellite variants. Chromosome-specific higher-order *CEN180* repetition is prevalent within the centromeres. We identified *ATHILA* retrotransposons that have invaded the satellite arrays and interrupt the genetic and epigenetic organization of the centromeres. By analyzing SPO11-1-oligonucleotide data from mutant lines, we demonstrate that DNA methylation epigenetically silences initiation of meiotic DNA double-strand breaks (DSBs) within the centromeres. Our data suggest that satellite homogenization and retrotransposon invasion are driving cycles of centromere evolution in *Arabidopsis*.

## Complete assembly of the *Arabidopsis* centromeres

We collected Col-0 genomic ONT and HiFi sequencing data comprising a total of 73.6 Gbp (~56×, >50 kbp) and 14.6 Gbp (111.3×, 15.6 kbp mean read length), respectively. These data yielded an improved assembly of the Col-0 genome (Col-CEN v1.2), where chromosomes 1, 3, and 5 are wholly resolved from telomere to telomere, and chromosomes 2 and 4 are complete apart from the short-arm 45*S* ribosomal DNA (rDNA) clusters and adjacent telomeres (Fig. 1). After telomere patching and repeat-aware polishing with ONT, HiFi, and Illumina reads (*15*), the Col-CEN assembly has a quality value of 45.99 and 51.71 inside and outside of the centromeres, equivalent to approximately one error per 40,000 and 148,000 bases, respectively (figs. S1 and S2A and table S1). Additionally, Hi-C and Bionano optical maps validate the large-scale structural accuracy of the assembly (fig. S2). The Col-CEN assembly is highly concordant with TAIR10, showing no large structural differences within the chromosome arms (Fig. 1B). Of the Col-0 bacterial artificial chromosome (BAC) contigs, 97.5% align to both TAIR10 and Col-CEN with high coverage and identity (>95%), and 99.9% of TAIR10 gene annotations are represented in Col-CEN.

Col-CEN reconstructs all five centromeres spanning 12.6 Mbp of new sequence, 120.0 and 97.6 kbp of 45*S* rDNA in the chromosome 2 and 4 nucleolar organizer regions (NORs), and

[1]Department of Plant Sciences, Downing Street, University of Cambridge, Cambridge CB2 3EA, UK. [2]Department of Computer Science, Johns Hopkins University, Baltimore, MD, USA. [3]The Plant Molecular and Cellular Biology Laboratory, Salk Institute for Biological Studies, La Jolla, CA, USA. [4]Gregor Mendel Institute (GMI), Austrian Academy of Sciences, Vienna BioCenter (VBC), Dr. Bohr-Gasse 3, 1030 Vienna, Austria. [5]Central European Institute of Technology (CEITEC), Masaryk University, Kamenice 5, Brno 625 00, Czech Republic. [6]School of Biosciences and Institute for Sustainable Food, University of Sheffield, Sheffield S10 2TN, UK. [7]Department of Biological Sciences, University of Tokyo, Tokyo, Japan. [8]Howard Hughes Medical Institute, Cold Spring Harbor Laboratory, Cold Spring Harbor, NY, USA. [9]Faculty of Biology, LMU Munich, Großhaderner Str. 2, 82152 Planegg-Martinsried, Germany. [10]Department of Chromosome Biology, Max Planck Institute for Plant Breeding Research, Carl-von-Linné-Weg 10, 50829 Cologne, Germany. [11]School of Life Sciences, University of Sussex, Brighton BN1 9RH, UK.
***Corresponding author. Email: mschatz@cs.jhu.edu (M.C.S.); irh25@cam.ac.uk (I.R.H.)**
†These authors contributed equally to this work.

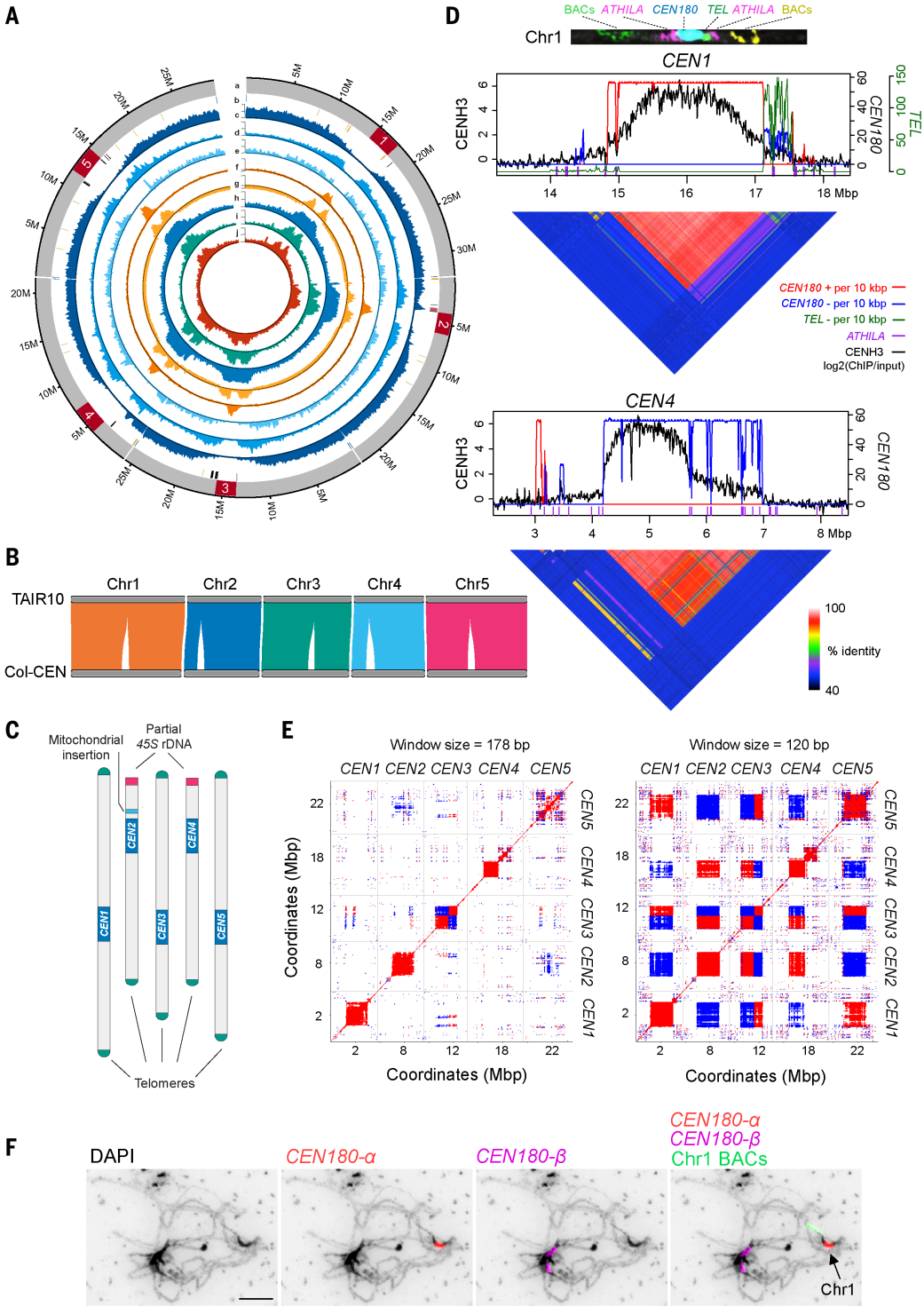


**Fig. 1. Complete assembly of the *Arabidopsis* centromeres.** (**A**) Circos plot of the Col-CEN assembly. Quantitative tracks (labeled c to j) are aggregated in 100-kbp bins, and independent *y*-axis labels are given as (low value, mid value, high value, measurement unit) as follows: (a) chromosome with centromeres shown in red; (b) telomeres (blue), 45*S* rDNA (yellow), 5*S* rDNA (black), and the mitochondrial insertion (pink); (c) genes (0, 25, 51, gene number); (d) transposable elements (0, 84, 167, transposable element number); (e) Col×Ler $F_2$ crossovers (0, 7, 14, crossover number); (f) CENH3 [−0.5, 0, 3, $\log_2$(ChIP/input)]; (g) H3K9me2 [−0.6, 0, 2, $\log_2$(ChIP/input)]; (h) CG methylation (0, 47, 95, %); (i) CHG methylation (0, 28, 56, %); and (j) CHH methylation (0, 7, 13, %). (**B**) Syntenic alignments between the TAIR10 and Col-CEN assemblies. (**C**) Col-CEN ideogram with annotated chromosome landmarks (not drawn to scale). (**D**) CENH3 $\log_2$(ChIP/input) (black) plotted over centromeres 1 and 4 (*10*). *CEN180* per 10-kbp plotted for forward (red) or reverse (blue) strand orientations. *ATHILA* are indicated by purple *x*-axis ticks. Heatmaps show pairwise sequence identity between all nonoverlapping 5-kbp regions. A FISH-stained chromosome 1 at pachytene is shown at the top, probed with upper-arm BACs (green), *ATHILA* (purple), *CEN180* (blue), the telomeric repeat (green), and bottom-arm BACs (yellow). (**E**) Dot plots comparing the five centromeres using a search window of 120 or 178 bp. Red and blue indicate forward- and reverse-strand similarity, respectively. (**F**) Pachytene-stage chromosomes stained with 4′,6-diamidino-2-phenylindole (DAPI) (black) and *CEN180*-α (red), *CEN180*-β (purple), and chromosome 1 BAC (green) FISH probes. The scale bar represents 10 μM.

the complete telomeres of the eight chromosome arms without subtelomeric NORs (Fig. 1, A to C; and figs. S1 to S3). We found several instances of apparently genuine variation between the Col-0 strains used to generate TAIR10 and Col-CEN (fig. S4 and tables S2 and S3). For example, a thionin gene cluster shows a deletion in Col-CEN relative to TAIR10 (fig. S4). In total, 27 TAIR10 genes are missing from Col-CEN owing to presence or absence variation, and 13 are present in multiple copies (tables S2 and S3). To comprehensively account for variation between Col-0 strains, we aligned ONT, HiFi, and Illumina reads to the Col-CEN assembly and called variants, providing a database of potential allelic differences, including heterozygous variants (https://github.com/schatzlab/Col-CEN). This revealed only 41 and 37 structural variant calls from ONT and HiFi data genome-wide, respectively, consistent with very low heterozygosity.

We confirmed chromosome landmarks flanking centromere 1 using fluorescence in situ hybridization (FISH), which included labeling a telomeric-repeat cluster located adjacent to the centromere (Fig. 1D and fig. S5). To validate centromere structure, we performed in silico

digestion with AscI and NotI and compared the predicted fragments with published physical maps, which validated Col-CEN (fig. S6) (*16*). We also examined our Bionano optical data across the centromeres (fig. S7). The optical contigs are consistent with the structure of Col-CEN *CEN180* arrays, although the low density of centromeric labeling sites prevents full resolution by optical fragments alone (fig. S7).

The centromeres are characterized by a 178-bp satellite repeat (*CEN180*), arranged head to tail and organized into higher-order repeats (Figs. 1D and 2 and fig. S8). We validated the structural and base-level accuracy of the centromeres using techniques from the human Telomere-to-Telomere (T2T) Consortium (*6*, *8*) and observed even long-read coverage across the centromeres with few loci showing plausible alternate base signals (fig. S1B). We observed relatively few missing *k*-mers that are found in the assembly but not in Illumina short reads, which are diagnostic of residual consensus errors that remain after polishing (fig. S1B) (*17*). We observed that unique marker sequences are frequent, with a maximum distance between consecutive markers of 41,765 bp within the centromeres, suggesting that our reads can confidently span these markers and assemble reliably (fig. S1C). The five centromeres are relatively distinct at the sequence level, with each exhibiting chromosome-specific repeats (Figs. 1E and 2 and tables S4 and S5). Using the Col-CEN sequence, we designed *CEN180* variant FISH probes to label specific centromere arrays (Fig. 1F and fig. S5). For example, the *CEN180*-α, *CEN180*-γ, and *CEN180*-δ probes specifically label arrays within centromere 1 (Fig. 1F and fig. S5), providing cytogenetic validation for chromosome-specific satellites.

### The *Arabidopsis CEN180* satellite repeat library

We performed de novo searches for tandem repeats to define the centromere satellite library (table S4). We identified 66,131 *CEN180* satellites in total, with between 11,848 and 15,613 copies per chromosome (Fig. 2, fig. S9, and table S4). The *CEN180* repeats form large tandem arrays, with the satellites within each centromere found predominantly on the same strand, except for centromere 3, which is formed of two blocks on opposite strands (Fig. 1D and fig. S8). The distribution of repeat monomer length is constrained around 178 bp (Fig. 2A and fig. S9). We aligned all *CEN180* sequences to derive a genome-wide consensus and calculated nucleotide frequencies at each alignment position to generate a position probability matrix (PPM). Each satellite was compared with the PPM to calculate a "variant distance" by summation of disagreeing nucleotide probabilities. Substantial sequence variation was observed between satellites and the PPM, with a mean variant distance of 20.2 (Fig. 2A). Each centromere contains essentially private libraries of *CEN180* monomers, with only 0.3% sharing an identical copy on a different chromosome (Fig. 1E and table S4). By contrast, there is a high degree of *CEN180* repetition within chromosomes, with 57.1 to 69.0% showing one or more duplicates (table S4). We also observed a minor class of *CEN160* repeats found on chromosome 1 (1289 repeats, mean length of 158.2 bp) (*14*).

We aligned CENH3 chromatin immunoprecipitation sequencing (ChIP-seq) data to the Col-CEN assembly and observed, on average, 12.9-fold $\log_2$(ChIP/input) enrichment within the *CEN180* arrays, compared with the chromosome arms (Fig. 1D and fig. S8) (*10*). CENH3 ChIP-seq enrichment is generally highest within the interior of the main *CEN180* arrays (Fig. 1D and fig. S8). We observed a negative relationship between CENH3 ChIP-seq enrichment and *CEN180* variant distance (Fig. 2, D and E), consistent with the idea that CENH3 nucleosomes prefer to occupy satellites that are closer to the genome-wide consensus. In this respect, centromere 4 is noteworthy because it consists of two distinct *CEN180* arrays, with the right array showing higher variant distances and lower CENH3 enrichment (Figs. 1D and 2D and fig. S8). Together, these data are consistent with the possibility that satellite divergence leads to loss of CENH3 binding, or vice versa.

To define *CEN180* higher-order repeats, monomers were considered the same if they shared five or fewer pairwise variants. Consecutive repeats of at least two monomers below this variant threshold were identified, yielding 2,408,653 higher-order repeats (Fig. 2D and table S5). Like the *CEN180* monomer sequences, higher-order repeats are largely chromosome specific (table S5). The mean number of *CEN180* monomers per higher-order repeat was 2.41 (equivalent to 429 bp) (Fig. 2B and table S5), and 95.4% of *CEN180* were monomers of at least one larger repeat unit. Higher-order repeat block sizes show a negative exponential distribution, and the largest block was formed of 60 monomers (equivalent to 10,689 bp) (Fig. 2B). Many higher-order repeats are in close proximity (26% are <100 kbp apart), although they are dispersed throughout the length of the centromeres. For example, the average distance between higher-order repeats was 380 kbp and the maximum was 2365 kbp (Fig. 2B and table S5). We also observed that higher-order repeats further apart showed a higher level of variants between the blocks (variants per monomer) (Fig. 2F), consistent with the idea that satellite homogenization is more effective over repeats that are physically closer. Genome-wide, the *CEN180* quantile with highest CENH3 occupancy correlates with higher-order repetition and increased CG DNA methylation (Fig. 2, D, E, and G). However, an exception to these trends is centromere 5, which has 6.8 to 13.4% of higher-order repeats compared with the other centromeres yet recruits comparable CENH3 (Fig. 2G and table S5).

### Invasion of the *Arabidopsis* centromeres by *ATHILA* retrotransposons

In addition to reduced *CEN180* higher-order repetition, centromere 5 is also disrupted by breaks in the satellite array (Fig. 2G and fig. S8). Most of the main satellite arrays are *CEN180* (92.8%), with only 111 interspersed sequences >1 kbp. Within these breaks, we identified 53 intact and 20 fragmented *ATHILA* long terminal repeat (LTR) retrotransposons of the *GYPSY* superfamily (Fig. 3, A to C, and table S6) (*18*). The intact *ATHILA* have a mean length of 11.05 kbp, and most have similar and paired LTRs, target site duplications, primer binding sites, polypurine tracts, and *GYPSY* open reading frames (Fig. 3C and table S6). LTR comparisons indicate that the centromeric *ATHILA* are young, with, on average, 98.7% LTR sequence identity, which was significantly higher than that for *ATHILA* located outside the centromeres (96.9%, $n = 58$, Wilcox test, $P = 4.89 \times 10^{-8}$) (Fig. 3D and fig. S10). We also identified 12 *ATHILA* solo LTRs, consistent with postintegration intra-element homologous recombination (table S6). We observed six instances where centromeric *ATHILA* loci were duplicated on the same chromosome and located between 8.9 and 538.5 kbp apart, consistent with the idea that transposons are copied postintegration, potentially by the same mechanism that generates *CEN180* higher-order repeats. For example, a pair of adjacent *ATHILA5* and *ATHILA6A* elements within centromere 5 has been duplicated within a higher-order repeat (fig. S11). The duplicated elements share target site duplications and flanking sequences and show high identity between copies (99.5 and 99.6%) (fig. S11 and table S6). By contrast, the surrounding *CEN180* show higher divergence and copy number variation between the higher-order repeats (94.3 to 97.3% identity) (fig. S11). This indicates an increased rate of *CEN180* sequence change compared with that of the *ATHILA*, after duplication.

We analyzed centromeric *ATHILA* for CENH3 ChIP-seq enrichment and observed a decrease relative to the surrounding *CEN180*, yet higher levels than in *ATHILA* located outside of the centromere (Fig. 3E). The *ATHILA* show greater histone H3 lysine 9 dimethylation (H3K9me2) enrichment compared with all *CEN180* (Fig. 3E). We used our ONT reads to profile DNA methylation over the *ATHILA* and observed dense methylation, with higher CHG-context methylation (where H is A, T, or C) than the

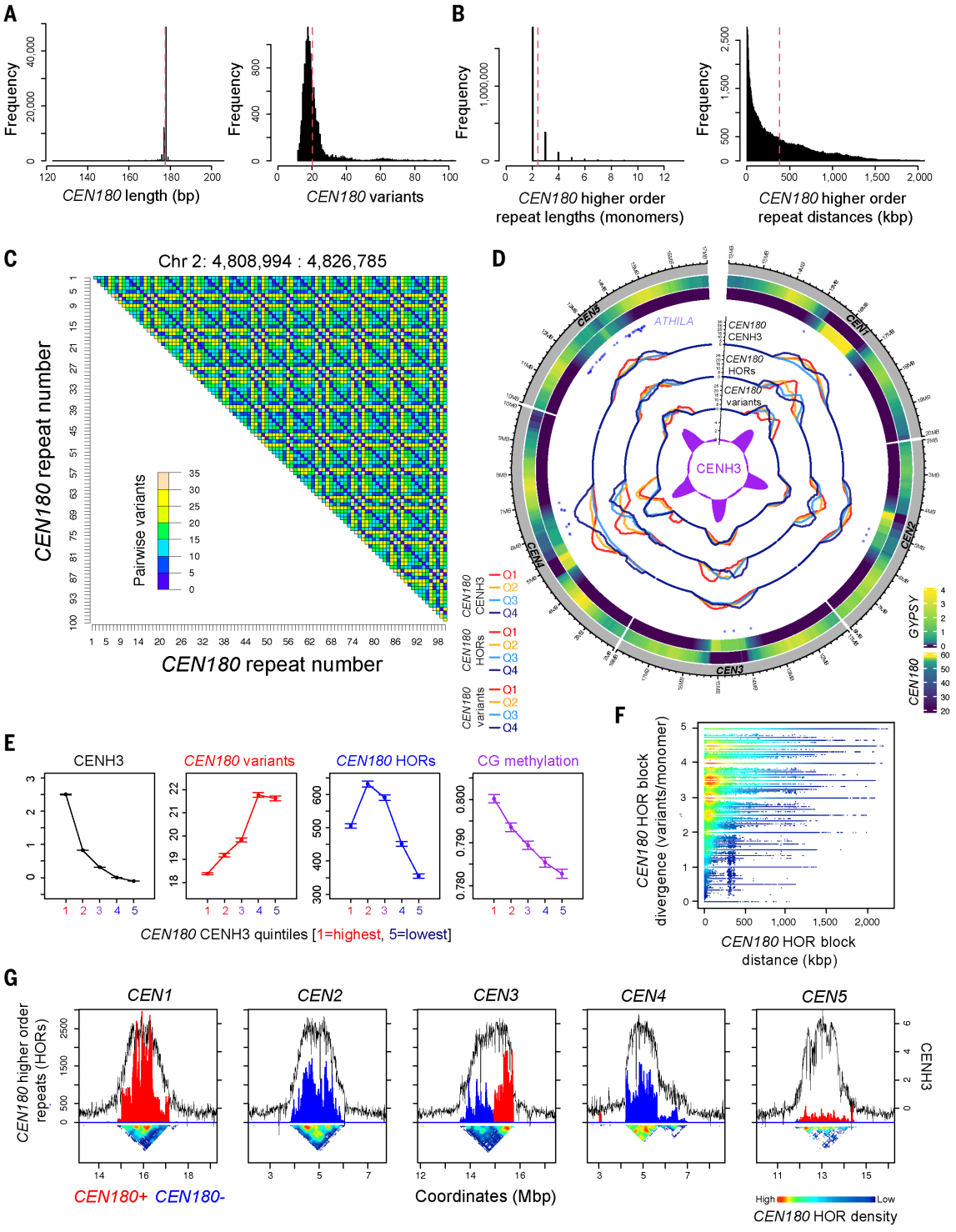


**Fig. 2. The *Arabidopsis CEN180* satellite repeat library.** (**A**) Histograms of *CEN180* monomer lengths (bp), and variant distances relative to the genome-wide consensus. Red dashed lines indicate mean values. (**B**) Same as for (A) but showing widths of *CEN180* higher-order repeat blocks (monomers) and the distance between higher-order repeats (kbp). (**C**) Heatmap of a representative region within centromere 2, shaded according to pairwise variants between *CEN180*. (**D**) Circos plot showing (i) *GYPSY* density; (ii) *CEN180* density; (iii) centromeric *ATHILA* "rainfall"; (iv) *CEN180* density grouped by decreasing CENH3 $\log_2$(ChIP/input) (red, high; navy, low); (v) *CEN180* density grouped by decreasing higher-order repetition (red, high; navy, low); (vi) *CEN180* grouped by decreasing variant distance (red, high; navy, low); and (vii) CENH3 $\log_2$(ChIP/input) (purple) across the centromeres. (**E**) *CEN180* were divided into quintiles according to CENH3 $\log_2$(ChIP/input) and mean values with 95% confidence intervals plotted. The same groups were analyzed for *CEN180* variant distance (red), higher-order repetition (blue), and CG-context DNA methylation (purple). (**F**) Plot of the distance between pairs of higher-order repeats (kbp) and divergence (variants per monomer) between the higher-order repeats. (**G**) Plots of CENH3 $\log_2$(ChIP/input) (black) across the centromeres compared with *CEN180* higher-order repetition on forward (red) or reverse (blue) strands. The heatmap beneath is shaded according to higher-order repeat density.

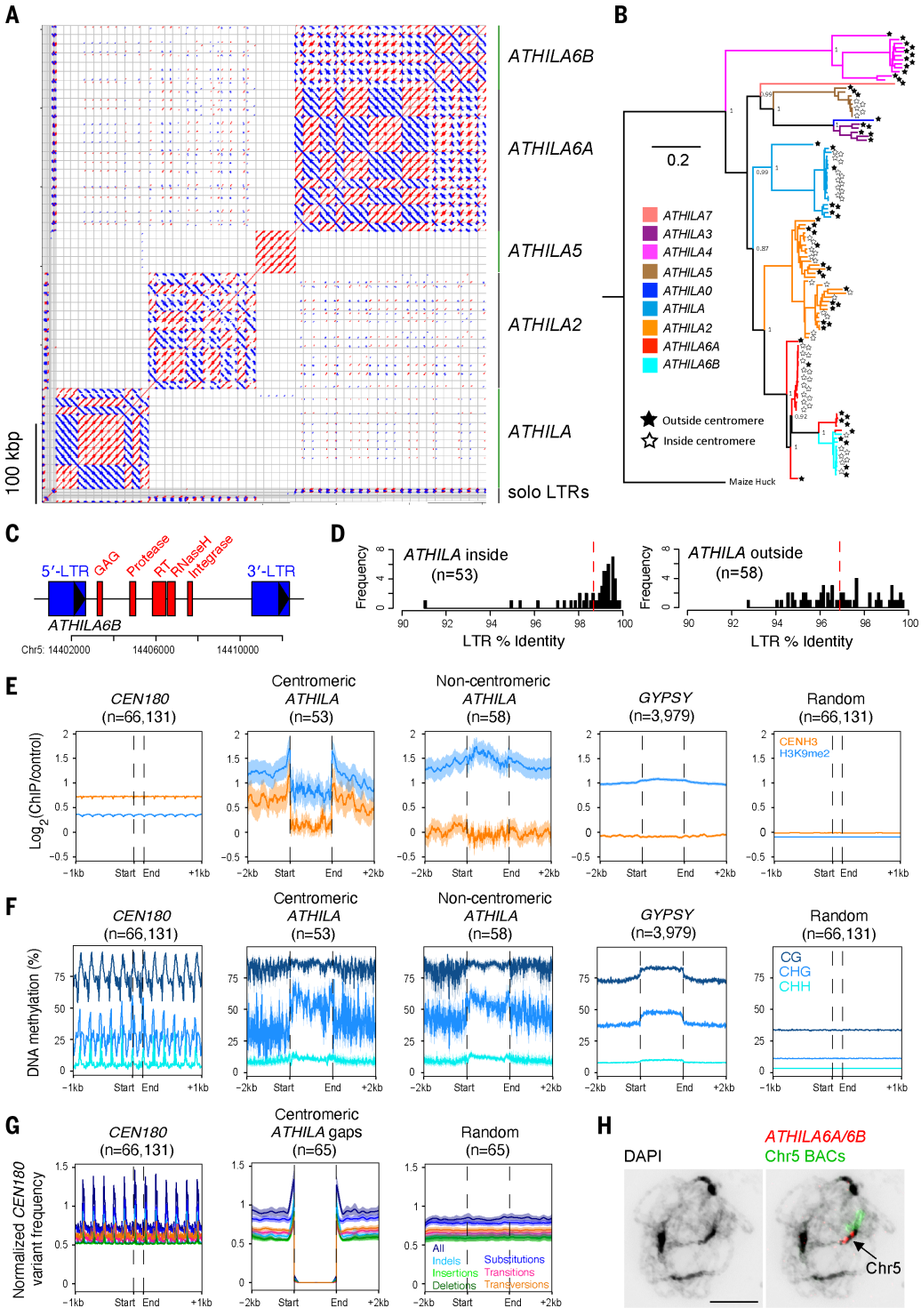


**Fig. 3. Invasion of the *Arabidopsis* centromeres by *ATHILA* retrotransposons.** (**A**) Dot plot of centromeric *ATHILA* using a 50-bp search window. Red and blue indicate forward- and reverse-strand similarity, respectively. *ATHILA* subfamilies and solo LTRs are indicated. (**B**) Maximum likelihood phylogenetic tree of 111 intact *ATHILA* elements, color coded according to subfamily. Stars at the branch tips indicate *ATHILA* inside (white) or outside (black) the centromeres. (**C**) An annotated map of an *ATHILA6B* with LTRs (blue) and core protein domains (red) highlighted. (**D**) Histograms of LTR sequence identity for centromeric *ATHILA* elements ($n$ = 53) compared with *ATHILA* outside of the centromeres ($n$ = 58). Red dashed lines indicate mean values. (**E**) Metaprofiles of CENH3 (orange) and H3K9me2 (blue) ChIP-seq signals around *CEN180* ($n$ = 66,131), centromeric intact *ATHILA* ($n$ = 53), *ATHILA* located outside the centromeres ($n$ = 58), *GYPSY* retrotransposons ($n$ = 3979), and random positions ($n$ = 66,131). Shaded ribbons represent 95% confidence intervals for windowed mean values. (**F**) Same as for (E) but analyzing ONT-derived percentage of DNA methylation in CG (dark blue), CHG (blue), and CHH (light blue) contexts. (**G**) Metaprofiles of *CEN180* sequence edits (insertions, deletions, and substitutions relative to the *CEN180* consensus), normalized by *CEN180* presence, in positions surrounding *CEN180* gaps containing *ATHILA* ($n$ = 65) or random positions ($n$ = 65). All edits (dark blue), substitutions (blue), indels (light blue), insertions (light green), deletions (dark green), transitions (pink), and transversions (orange) are shown. Shaded ribbons represent 95% confidence intervals for windowed mean values. (**H**) Pachytene-stage chromosome spread stained with DAPI (black), an *ATHILA6A/6B GAG* FISH probe (red), and chromosome 5–specific BACs (green). The scale bar represents 10 μM.

surrounding *CEN180* (Fig. 3F). Hence, *ATHILA* elements are distinct from the *CEN180* satellites at the chromatin level. We profiled *CEN180* variants around centromeric *ATHILA* loci ($n$ = 65) and observed increased satellite divergence in the flanking regions (Fig. 3G), reminiscent of *Nasonia PSR* tandem repeat divergence at the junction with a *NATE* retrotransposon (*19*). This indicates that *ATHILA* insertion was mutagenic on the surrounding satellites or that transposon insertion influenced the subsequent divergence or homogenization of the adjacent *CEN180*. We also used FISH to cytogenetically validate the presence of *ATHILA6A/6B* and *ATHILA2* subfamilies within the centromeres (Fig. 3H and fig. S5). Together, these data show that *ATHILA* insertions interrupt the genetic and epigenetic organization of the *Arabidopsis CEN180* arrays.

### Epigenetic organization and meiotic recombination within the centromeres

To assess genetic and epigenetic features of the centromeres, we analyzed all of the chromosome arms along their telomere-centromere axes using a proportional scale (Fig. 4A). Centromere midpoints were defined as the point of maximum CENH3 ChIP-seq enrichment (fig. S12). As expected, *CEN180* satellites are highly

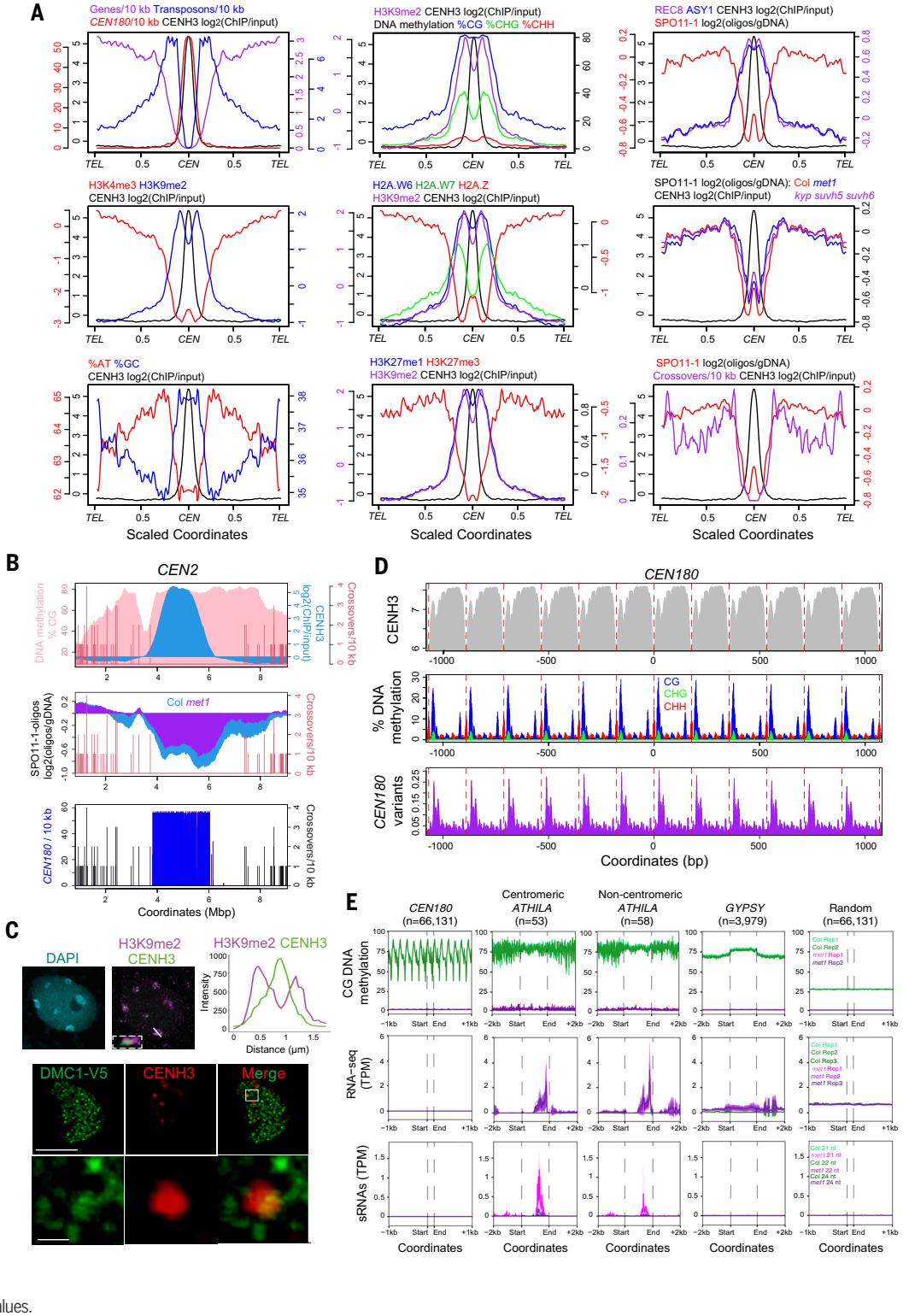


**Fig. 4. Epigenetic organization and meiotic recombination within the centromeres.** (**A**) Quantification of genomic features plotted along chromosome arms that were proportionally scaled between telomeres (*TEL*) and centromere midpoints (*CEN*) [defined by maximum CENH3 ChIP-seq $\log_2$(ChIP/input) enrichment]. Data analyzed were gene, transposon, and *CEN180* density; CENH3, H3K4me3, H3K9me2, H2A.W6, H2A.W7, H2A.Z, H3K27me1, H3K27me3, REC8, and ASY1 $\log_2$ (ChIP/input); and percentage of AT/GC base composition, DNA methylation, SPO11-1-oligonucleotides (in wild type and *met1*), and crossovers (table S7). (**B**) Plot quantifying crossovers (red), percentage of CG DNA methylation (pink), CENH3 (blue), SPO11-1-oligonucleotides in wild type and *met1*, and *CEN180* density along centromere 2. (**C**) An interphase nucleus immunostained for H3K9me2 (magenta) and CENH3-GFP (green) is shown at the top. The white line indicates the confocal section used for the intensity plot shown on the right; the region outlined by the white dashed line shows a magnified image of a centromere. The scale bar represents 5 μM. At the bottom is a male meiocyte (early prophase I) immunostained for CENH3 (red) and V5-DMC1 (green). The region outlined by the white line indicates the magnified region shown in the lower row of images. Scale bars are 10 μM (upper) and 1 μM (lower). (**D**) Plots of CENH3 ChIP enrichment (gray), DNA methylation in CG (blue), CHG (green) and CHH (red) contexts, and *CEN180* variants (purple), averaged over windows centered on *CEN180* starts. The red dashed lines show 178-bp increments. (**E**) Metaprofiles of CG-context DNA methylation, RNA-seq, and siRNA-seq in wild type (green) or *met1* (pink and purple) (*29*) around *CEN180* ($n$ = 66,131), centromeric intact *ATHILA* ($n$ = 53), *ATHILA* located outside the centromeres ($n$ = 58), *GYPSY* ($n$ = 3979), and random positions ($n$ = 66,131). Shaded ribbons represent 95% confidence intervals for windowed mean values.

enriched in proximity to centromeres, and these regions are relatively GC-rich compared with the AT-rich chromosome arms (Fig. 4A). Gene density drops as the centromeres are approached, whereas transposon density increases, until they are replaced by *CEN180* (Fig. 4A). Gene and transposon densities are tracked closely by H3K4me3 and H3K9me2 ChIP-seq enrichment, respectively (Fig. 4A). H3K9me2 enrichment is observed within the centromere, although there is a reduction in the center coincident with CENH3 enrichment (Fig. 4A), consistent with reduced H3 occupancy caused by CENH3 replacement. A slight increase in H3K4me3 enrichment is observed within the centromeres, relative to the flanking pericentromeres (Fig. 4A).

Using our ONT reads with the DeepSignal-plant algorithm (*20*), we observed dense DNA methylation across the centromeres in CG, CHG, and CHH contexts (Fig. 4, A and B). However, CHG DNA methylation shows relatively

reduced centromeric frequency compared with CG methylation (Fig. 4A). This may reflect centromeric depletion of H3K9me2 (Fig. 4A), a histone modification that maintains DNA methylation in non-CG contexts (*21*). To further investigate the DNA methylation environment associated with CENH3 deposition, we performed ChIP using either H3K9me2 or CENH3 antibodies and sequenced the immunopurified DNA with ONT. We analyzed methylation frequency in reads that aligned to the centromeres and observed dense CG methylation in both read sets but depletion of CHG and CHH methylation in the CENH3 reads relative to H3K9me2 (fig. S13). This further supports that H3 replacement by CENH3 causes a decrease in non-CG methylation maintenance within the *Arabidopsis* centromeres.

To investigate genetic control of centromeric DNA methylation, we analyzed bisulfite sequencing (BS-seq) data from wild type and eight mutants defective in CG and non-CG DNA methylation maintenance (fig. S14) (*21*, *22*). Centromeric non-CG methylation is eliminated in *drm1 drm2 cmt2 cmt3* mutants and reduced in *kyp suvh5 suvh6* mutants, whereas CG methylation is intact in these backgrounds (fig. S14) (*21*, *22*). By contrast, both CG and non-CG methylation in the centromeres are reduced in *ddm1* and *met1* mutants (fig. S14) (*22*). Hence, centromeric CG-context methylation is relatively high compared with non-CG, and non-CG methylation shows an unexpected dependence on CG maintenance pathways.

We observed pericentromeric ChIP-seq enrichment of the heterochromatic marks H2A.W6, H2A.W7, and H3K27me1, which are relatively depleted within the centromeres (Fig. 4A) (*23*, *24*). The polycomb-group modification H3K27me3 is low in the centromeres and found largely in the chromosome arms (Fig. 4A). Enrichment of the euchromatic histone variant H2A.Z is low in the centromeres, but, like H3K4me3, shows a slight increase in the centromeres relative to the pericentromeres (Fig. 4A), suggesting that the centromeres have a distinct chromatin state relative to neighboring heterochromatin. We performed immunofluorescent staining of *Arabidopsis* nuclei for CENH3-GFP (GFP, green fluorescent protein) and euchromatic and heterochromatic histone modifications (Fig. 4C and figs. S15 and S16). Quantification of fluorescence intensity confirmed that heterochromatic marks are relatively depleted where CENH3-GFP is enriched (Fig. 4C and fig. S16). Hence, the *Arabidopsis* centromeres show depletion of heterochromatic and enrichment of euchromatic marks relative to the pericentromeres, consistent with a hybrid chromatin state.

Meiotic recombination, including unequal crossover and gene conversion, has been proposed to mediate centromere evolution (*4*, *25*). We mapped 2080 meiotic crossovers from Col×Ler $F_2$ sequencing data against the Col-CEN assembly (resolved, on average, to 1047 kbp) (fig. S17). As expected, crossovers were suppressed in proximity to the centromeres (Fig. 4, A and B, and fig. S17). We observed high centromeric ChIP-seq enrichment of REC8-cohesin and ASY1, which are components of the meiotic chromosome axis (Fig. 4A) (*26*, *27*). To investigate the potential for meiotic DSB formation within the centromeres, we aligned SPO11-1-oligonucleotides from wild type (*28*). Overall, SPO11-1-oligonucleotides are low within the centromeres, although we observed an increase relative to the pericentromeres, reminiscent of H3K4me3 and H2A.Z ChIP-seq enrichment (Fig. 4A). To investigate the role of DNA methylation, we mapped SPO11-1-oligonucleotides from the CG DNA methylation mutant *met1-3* (*28*), which showed a gain of DSBs within the centromeres (Fig. 4, A and B). We immunostained meiocytes in early prophase I for CENH3 and V5-DMC1, which is a marker of meiotic interhomolog recombination (Fig. 4C and figs. S18 and S19). DMC1-V5 foci were observed along the chromosomes and adjacent to the surface of CENH3 foci, but not within them (Fig. 4C). Hence, despite suppression of crossovers, we observe evidence for low levels of meiotic recombination initiation within the centromeres, which is influenced by DNA methylation.

CENH3 nucleosomes show a phased pattern of enrichment with the *CEN180*, with relative depletion in spacer regions at the satellite edges (Fig. 4D). CENH3 spacer regions also associate with increased DNA methylation and *CEN180* variants (Fig. 4D), consistent with the possibility that CENH3-nucleosomes influence epigenetic modification and satellite divergence. We analyzed chromatin and transcription around *CEN180* and *ATHILA* at the fine scale and compared wild type with the DNA methylation mutant *met1-3*. In *met1-3*, CG-context DNA methylation is lost in both *ATHILA* and *CEN180* repeats (Fig. 4E and fig. S20) (*29*). However, *met1* RNA sequencing (RNA-seq) and small interfering RNA sequencing (siRNA-seq) signals show increased expression of *ATHILA* transcripts, but not *CEN180* (Fig. 4E and fig. S20) (*29*). The greatest RNA and siRNA expression increases in *met1-3* are observed in the *ATHILA* internal 3′ regions (Fig. 4E and fig. S20), which correspond to transcriptionally silent information (TSI) transcripts and epigenetically activated siRNA (easiRNA) populations (*30*, *31*). This further indicates that epigenetic regulation of the *CEN180* repeats is distinct from that of the *ATHILA* elements.

## Discussion

Leveraging advances in sequencing technology and genome assembly, we have generated the Col-CEN reference genome, which resolves the centromere satellite arrays. By profiling chromatin and recombination within the centromeres, we demonstrate that Col-CEN enables biological insights from existing functional genomics data. Using ONT long reads, we have also resolved patterns of DNA methylation within the centromeres, highlighting the potential of complete reference assemblies for understanding epigenetic regulation of repeats. The Col-0 centromeres contain interspersed unique sequences that facilitate assembly with modern sequencing reads. However, similar to the human T2T Consortium, the Col-CEN assembly required extensive manual processes to polish and curate repetitive loci (*8*, *15*, *32*). We anticipate that as complete genome assembly becomes more automated, researchers will be able to compare centromere sequences across populations and species, ultimately revealing how centromere diversity and evolution affect genome function.

In the centromeres, extensive variation is observed among the *CEN180*, and most monomer sequences are private to each centromere. This is consistent with the model that satellite homogenization occurs primarily within chromosomes. The negative correlation between *CEN180* divergence and CENH3 occupancy suggests that centromeric chromatin may promote recombination pathways that lead to homogenization, including DSB formation and repair through homologous recombination. For example, interhomolog strand invasion and noncrossover repair during meiosis, using allelic or nonallelic templates, have the potential to cause *CEN180* gene conversion and structural change (fig. S21). Similarly, repair and recombination using a sister chromatid may also contribute to *CEN180* change, which could occur during mitosis or meiosis (fig. S21). We note that *CEN180* higher-order repeats are, on average, 432 bp long, which is within the size range of *Arabidopsis* gene conversions (*33*), although we also observe large (10 to 100 kbp) intra-centromere duplications, for which the origin is less clear. We observe a proximity effect on divergence between *CEN180* higher-order repeats, with repeat blocks that are further apart showing greater differences. These patterns are reminiscent of human centromeric higher-order repeats, although duplicated blocks of α-satellites are longer and occur over greater physical distances (*6*, *34*, *35*). Because meiotic crossover repair is suppressed within the centromeres, consistent with patterns across eukaryotes (*25*, *36*), we do not consider unequal crossover to be a major pathway driving *Arabidopsis* centromere evolution. However, we propose that a recombination-based homogenization process, occurring between allelic or nonallelic locations on the same chromosome, maintains the *CEN180* library close to

the consensus that is optimal for CENH3 recruitment (fig. S21).

Aside from homogenizing recombination within the *CEN180*, the centromeres have experienced invasion by *ATHILA* retrotransposons. The ability of *ATHILA* to insert within the centromeres is likely determined by their integrase protein. The Tal1 *COPIA* element from *Arabidopsis lyrata* also shows an insertion bias into *CEN180* when expressed in *A. thaliana (37)*, despite satellite sequences varying between these species (*38*), indicating that epigenetic information may be important for targeting. Most of the centromeric *ATHILA* elements appear young, based on high LTR identity, and possess many features required for transposition, although the centromeres show differences in the frequency of *ATHILA* insertions, with centromeres 4 and 5 being the most invaded. Compared with *CEN180*, centromeric *ATHILA* have distinct chromatin profiles and are associated with increased satellite divergence in adjacent regions. Therefore, *ATHILA* elements represent a potentially disruptive influence on the genetic and epigenetic organization of the centromeres. However, transposons are widespread in the centromeres of diverse eukaryotes and can directly contribute to repeat evolution (e.g., mammalian CENP-B is derived from a Pogo DNA transposase) (*39*). Therefore, *ATHILA* elements may also beneficially contribute to centromere integrity and stability in *Arabidopsis*.

The advantage conferred to *ATHILA* by integration within the centromeres is presently unclear, although we speculate that they may be engaged in centromere drive (*40*). Haig-Grafen scrambling through recombination has been proposed as a defense against drive elements within the centromeres (*41*). For example, maize meiotic gene conversion can eliminate centromeric *CRM2* retrotransposons (*25*). Therefore, centromere satellite homogenization may serve as a mechanism to purge *ATHILA*, although in some cases this results in transposon duplication (fig. S22). The presence of *ATHILA* solo LTRs is also consistent with homologous recombination acting on the retrotransposons after integration (fig. S22). Centromere 5 and the diverged *CEN180* array in centromere 4 show both high *ATHILA* density and reduced *CEN180* higher-order repetition. This indicates that *ATHILA* may inhibit *CEN180* homogenization or that loss of homogenization facilitates *ATHILA* insertion. We propose that each *Arabidopsis* centromere represents a different stage in cycles of satellite homogenization and *ATHILA*-driven diversification. These opposing forces provide a dual capacity for homeostasis and change during centromere evolution. Assembly of centromeres from multiple *Arabidopsis* accessions, and closely related species, has the potential to reveal new insights into centromere formation and the evolutionary dynamics of *CEN180* and *ATHILA* repeats.

## Methods summary

Genomic DNA was extracted from *A. thaliana* Col-0 plants and used for ONT and PacBio HiFi long-read sequencing and Bionano optical mapping. ONT reads were used to establish a draft assembly, which was then scaffolded and polished with HiFi reads to generate the Col-CEN v1.2 assembly. ONT reads were used to analyze DNA methylation with the DeepSignal-plant algorithm (*20*). *CEN180* monomers, higher-order repeats, and *ATHILA* retrotransposons were identified de novo using custom pipelines. Short-read datasets (table S7) were aligned to Col-CEN to map chromatin and recombination distributions, using standard methods. Cytogenetic analysis of the centromeres was performed using FISH and immunofluorescence staining. A full description of all experimental and computational methods can be found in the supplementary materials.

## REFERENCES AND NOTES


1. H. S. Malik, S. Henikoff, Major evolutionary transitions in centromere complexity. *Cell* **138**, 1067–1082 (2009). doi: 10.1016/j.cell.2009.08.036; pmid: 19766562
2. D. P. Melters *et al*., Comparative analysis of tandem repeats from hundreds of species reveals unique insights into centromere evolution. *Genome Biol.* **14**, R10 (2013). doi: 10.1186/gb-2013-14-1-r10; pmid: 23363705
3. K. L. McKinley, I. M. Cheeseman, The molecular basis for centromere identity and function. *Nat. Rev. Mol. Cell Biol.* **17**, 16–29 (2016). doi: 10.1038/nrm.2015.5; pmid: 26601620
4. M. K. Rudd, G. A. Wray, H. F. Willard, The evolutionary dynamics of α-satellite. *Genome Res.* **16**, 88–96 (2006). doi: 10.1101/gr.3810906; pmid: 16344556
5. M. Jain *et al*., Nanopore sequencing and assembly of a human genome with ultra-long reads. *Nat. Biotechnol.* **36**, 338–345 (2018). doi: 10.1038/nbt.4060; pmid: 29431738
6. K. H. Miga *et al*., Telomere-to-telomere assembly of a complete human X chromosome. *Nature* **585**, 79–84 (2020). doi: 10.1038/s41586-020-2547-7; pmid: 32663838
7. G. A. Logsdon *et al*., The structure, function and evolution of a complete human chromosome 8. *Nature* **593**, 101–107 (2021). doi: 10.1038/s41586-021-03420-7; pmid: 33828295
8. S. Nurk *et al*., The complete sequence of a human genome. *bioRxiv* 2021.05.26.445798 [Preprint] (2021). doi: 10.1101/2021.05.26.445798
9. Arabidopsis Genome Initiative, Analysis of the genome sequence of the flowering plant *Arabidopsis thaliana*. *Nature* **408**, 796–815 (2000). doi: 10.1038/35048692; pmid: 11130711
10. S. Maheshwari, T. Ishii, C. T. Brown, A. Houben, L. Comai, Centromere location in *Arabidopsis* is unaltered by extreme divergence in CENH3 protein sequence. *Genome Res.* **27**, 471–478 (2017). doi: 10.1101/gr.214619.116; pmid: 28223399
11. G. P. Copenhaver *et al*., Genetic definition and sequence analysis of *Arabidopsis* centromeres. *Science* **286**, 2468–2474 (1999). doi: 10.1126/science.286.5449.2468; pmid: 10617454
12. P. B. Talbert, R. Masuelli, A. P. Tyagi, L. Comai, S. Henikoff, Centromeric localization and adaptive evolution of an *Arabidopsis* histone H3 variant. *Plant Cell* **14**, 1053–1066 (2002). doi: 10.1105/tpc.010425; pmid: 12034896
13. J. M. Martinez-Zapater, M. A. Estelle, C. R. Somerville, A highly repeated DNA sequence in *Arabidopsis thaliana*. *Mol. Gen. Genet.* **204**, 417–423 (1986). doi: 10.1007/BF00331018
14. E. K. Round, S. K. Flowers, E. J. Richards, *Arabidopsis thaliana* centromere regions: Genetic map positions and repetitive DNA structure. *Genome Res.* **7**, 1045–1053 (1997). doi: 10.1101/gr.7.11.1045; pmid: 9371740
15. A. M. McCartney *et al*., Chasing perfection: validation and polishing strategies for telomere-to-telomere genome assemblies. *bioRxiv* 2021.07.02.450803 [Preprint] (2021). doi: 10.1101/2021.07.02.450803
16. T. Hosouchi, N. Kumekawa, H. Tsuruoka, H. Kotani, Physical map-based sizes of the centromeric regions of *Arabidopsis thaliana* chromosomes 1, 2, and 3. *DNA Res.* **9**, 117–121 (2002). doi: 10.1093/dnares/9.4.117; pmid: 12240833
17. A. Rhie, B. P. Walenz, S. Koren, A. M. Phillippy, Merqury: Reference-free quality, completeness, and phasing assessment for genome assemblies. *Genome Biol.* **21**, 245 (2020). doi: 10.1186/s13059-020-02134-9; pmid: 32928274
18. D. A. Wright, D. F. Voytas, *Athila4* of *Arabidopsis* and *Calypso* of soybean define a lineage of endogenous plant retroviruses. *Genome Res.* **12**, 122–131 (2002). doi: 10.1101/gr.196001; pmid: 11779837
19. B. F. McAllister, J. H. Werren, Evolution of tandemly repeated sequences: What happens at the end of an array? *J. Mol. Evol.* **48**, 469–481 (1999). doi: 10.1007/PL00006491; pmid: 10079285
20. P. Ni *et al*., Genome-wide detection of cytosine methylations in plant from nanopore sequencing data using deep learning. *bioRxiv* 2021.02.07.430077 [Preprint] (2021). doi: 10.1101/2021.02.07.430077
21. H. Stroud *et al*., Non-CG methylation patterns shape the epigenetic landscape in *Arabidopsis*. *Nat. Struct. Mol. Biol.* **21**, 64–72 (2014). doi: 10.1038/nsmb.2735; pmid: 24336224
22. H. Stroud, M. V. C. Greenberg, S. Feng, Y. V. Bernatavichute, S. E. Jacobsen, Comprehensive analysis of silencing mutants reveals complex regulation of the *Arabidopsis* methylome. *Cell* **152**, 352–364 (2013). doi: 10.1016/j.cell.2012.10.054; pmid: 23313553
23. Y. Jacob *et al*., ATXR5 and ATXR6 are H3K27 monomethyltransferases required for chromatin structure and gene silencing. *Nat. Struct. Mol. Biol.* **16**, 763–768 (2009). doi: 10.1038/nsmb.1611; pmid: 19503079
24. R. Yelagandula *et al*., The histone variant H2A.W defines heterochromatin and promotes chromatin condensation in *Arabidopsis*. *Cell* **158**, 98–109 (2014). doi: 10.1016/j.cell.2014.06.006; pmid: 24995981
25. J. Shi *et al*., Widespread gene conversion in centromere cores. *PLOS Biol.* **8**, e1000327 (2010). doi: 10.1371/journal.pbio.1000327; pmid: 20231874
26. C. Lambing *et al*., Interacting genomic landscapes of REC8-cohesin, chromatin, and meiotic recombination in *Arabidopsis*. *Plant Cell* **32**, 1218–1239 (2020). doi: 10.1105/tpc.19.00866; pmid: 32024691
27. C. Lambing, P. C. Kuo, A. J. Tock, S. D. Topp, I. R. Henderson, ASY1 acts as a dosage-dependent antagonist of telomere-led recombination and mediates crossover interference in *Arabidopsis*. *Proc. Natl. Acad. Sci. U.S.A.* **117**, 13647–13658 (2020). doi: 10.1073/pnas.1921055117; pmid: 32499315
28. K. Choi *et al*., Nucleosomes and DNA methylation shape meiotic DSB frequency in *Arabidopsis thaliana* transposons and gene regulatory regions. *Genome Res.* **28**, 532–546 (2018). doi: 10.1101/gr.225599.117; pmid: 29530928
29. M. Rigal *et al*., Epigenome confrontation triggers immediate reprogramming of DNA methylation and transposon silencing in *Arabidopsis thaliana* F1 epihybrids. *Proc. Natl. Acad. Sci. U.S.A.* **113**, E2083–E2092 (2016). doi: 10.1073/pnas.1600672113; pmid: 27001853
30. A. Steimer *et al*., Endogenous targets of transcriptional gene silencing in *Arabidopsis*. *Plant Cell* **12**, 1165–1178 (2000). doi: 10.1105/tpc.12.7.1165; pmid: 10899982
31. S. C. Lee *et al*., *Arabidopsis* retrotransposon virus-like particles and their regulation by epigenetically activated small RNA. *Genome Res.* **30**, 576–588 (2020). doi: 10.1101/gr.259044.119; pmid: 32303559
32. A. Rhie *et al*., Towards complete and error-free genome assemblies of all vertebrate species. *Nature* **592**, 737–746 (2021). doi: 10.1038/s41586-021-03451-0; pmid: 33911273
33. E. Wijnker *et al*., The genomic landscape of meiotic crossovers and gene conversions in *Arabidopsis thaliana*. *eLife* **2**, e01426 (2013). doi: 10.7554/eLife.01426; pmid: 24347547
34. S. J. Durfy, H. F. Willard, Patterns of intra- and interarray sequence variation in alpha satellite from the human X chromosome: Evidence for short-range homogenization of tandemly repeated DNA sequences. *Genomics* **5**, 810–821 (1989). doi: 10.1016/0888-7543(89)90123-7; pmid: 2591964
35. N. Altemose *et al*., Complete genomic and epigenetic maps of human centromeres. *bioRxiv* 2021.07.12.452052 [Preprint] (2021). doi: 10.1101/2021.07.12.452052
36. M. M. Mahtani, H. F. Willard, Physical and genetic mapping of the human X chromosome centromere: Repression of recombination. *Genome Res.* **8**, 100–110 (1998). doi: 10.1101/gr.8.2.100; pmid: 9477338

37. S. Tsukahara *et al*., Centromere-targeted de novo integrations of an LTR retrotransposon of *Arabidopsis lyrata*. *Genes Dev.* **26**, 705–713 (2012). doi: 10.1101/gad.183871.111; pmid: 22431508
38. A. Kawabe, S. Nasuda, Structure and genomic organization of centromeric repeats in *Arabidopsis* species. *Mol. Genet. Genomics* **272**, 593–602 (2005). doi: 10.1007/s00438-004-1081-x; pmid: 15586291
39. S. J. Klein, R. J. O'Neill, Transposable elements: Genome innovation, chromosome diversity, and centromere conflict. *Chromosome Res.* **26**, 5–23 (2018). doi: 10.1007/s10577-017-9569-5; pmid: 29332159
40. H. S. Malik, The centromere-drive hypothesis: A simple basis for centromere complexity. *Prog. Mol. Subcell. Biol.* **48**, 33–52 (2009). doi: 10.1007/978-3-642-00182-6_2; pmid: 19521811
41. D. Haig, A. Grafen, Genetic scrambling as a defence against meiotic drive. *J. Theor. Biol.* **153**, 531–558 (1991). doi: 10.1016/S0022-5193(05)80155-9; pmid: 1806752

## ACKNOWLEDGMENTS

This paper is dedicated to Simon Chan. We thank I. Thompson for *ATHILA* analysis, S. Henikoff for the generous gift of CENH3 antibodies, A. Shumate for help with gene Liftoff interpretation, B. Fischer for advice on high–molecular weight DNA isolation, and M. Pouch for assistance designing FISH probes. **Funding:** This work was supported by BBSRC grants BB/S006842/1, BB/S020012/1, and BB/V003984/1 to I.R.H.; European Research Council Consolidator Award ERC-2015-CoG-681987 "SynthHotSpot" to I.R.H.; Marie Curie International Training Network "MEICOM" to I.R.H.; Human Frontier Science Program award RGP0025/2021 to T.K., M.C.S., and I.R.H.; US National Institutes of Health grant S10OD028632-01; US National Science Foundation grants DBI-1350041 and IOS-1732253 to M.C.S.; Royal Society awards UF160222 and RGF/R1/180006 to A.B.; the Czech Science Foundation grant no. 21-03909S to M.A.L.; the Gregor Mendel Institute to F.B.; grants Fonds zur Förderung der wissenschaftlichen Forschung (FWF) P26887, P28320, P30802, P32054, and TAI304 to F.B. and chromatin dynamics W1238 to A.S. and B.J.; Leverhulme Trust Research Leadership grant RL-2012-042 to J.T.; and grants from the Howard Hughes Medical Institute and US National Institutes of Health (RO1GM067014) to R.A.M. **Author contributions:** M.N. sequenced DNA; performed genome assembly and analysis, ChIP-seq, and DNA methylation analysis; and wrote the manuscript. M.A. performed genome assembly, polishing, validation, annotation, and analysis and wrote the manuscript. P.W. performed satellite repeat annotation and genome analysis and wrote the manuscript. A.J.T. performed short-read alignment and genome analysis and wrote the manuscript. B.W.A. sequenced DNA, performed optical mapping, and contributed to the assembly. A.S. performed chromatin immunofluorescence analysis. B.J. provided ChIP-seq data. C.L. and P.K. performed immunocytology. N.Y. generated the DMC1 epitope-tagged line. N.H. and K.C. sequenced DNA and contributed to the assembly. L.M.S., J.T., and K.S. performed PacBio sequencing. T.K. and R.A.M. provided intellectual input. T.M. and M.A.L. performed FISH. F.B. supervised ChIP-seq and immunofluorescence analysis and wrote the manuscript. A.B. performed *ATHILA* annotation and genome analysis and wrote the manuscript. T.P.M. supervised DNA sequencing and genome assembly and analysis and wrote the manuscript. M.C.S. supervised genome assembly, validation, annotation, and analysis and wrote the manuscript. I.R.H. supervised DNA sequencing, genome assembly, validation, annotation, and analysis and wrote the manuscript. **Competing interests:** The authors have no competing interests. **Data and materials availability:** The ONT sequencing reads used for assembly are available for download at ArrayExpress accession E-MTAB-10272 (www.ebi.ac.uk/arrayexpress/). The PacBio HiFi reads are available for download at European Nucleotide Archive accession number PRJEB46164 (www.ebi.ac.uk/ena/browser/view/PRJEB46164). All data, code and materials are available in the manuscript or the supplementary materials and at https://github.com/schatzlab/Col-CEN.

## SUPPLEMENTARY MATERIALS

science.org/doi/10.1126/science.abi7489
Materials and Methods
Figs. S1 to S22
Tables S1 to S8
References (*42*–*94*)
MDAR Reproducibility Checklist

View/request a protocol for this paper from *Bio-protocol*.

31 March 2021; resubmitted 5 August 2021
Accepted 27 September 2021
10.1126/science.abi7489

Science

# The genetic and epigenetic landscape of the *Arabidopsis* centromeres

Matthew NaishMichael AlongePiotr WlodzimierzAndrew J. TockBradley W. AbramsonAnna SchmückerTerezie MandákováBhagyshree JamgeChristophe LambingPallas KuoNatasha YelinaNolan HartwickKelly ColtLisa M. SmithJurriaan TonTetsuji KakutaniRobert A. MartienssenKorbinian SchneebergerMartin A. LysakFrédéric BergerAlexandros BousiosTodd P. MichaelMichael C. SchatzIan R. Henderson

*Science*, 374 (6569), eabi7489. • DOI: 10.1126/science.abi7489

**A closer look at centromeres**

Centromeres are key for anchoring chromosomes to the mitotic spindle, but they have been difficult to sequence because they can contain many repeating DNA elements. These repeats, however, carry regularly spaced, distinctive sequence markers because of sequence heterogeneity between the mostly, but not completely, identical DNA sequence repeats. Such differences aid sequence assembly. Naish *et al*. used ultra-long-read DNA sequencing to establish a reference assembly that resolves all five centromeres in the small mustard plant *Arabidopsis*. Their view into the subtly homogenized world of centromeres reveals retrotransposons that interrupt centromere organization and repressive DNA methylation that excludes centromeres from meiotic crossover repair. Thus, *Arabidopsis* centromeres evolve under the opposing forces of sequence homogenization and retrotransposon disruption. —PJH







*Science* (ISSN ) is published by the American Association for the Advancement of Science. 1200 New York Avenue NW, Washington, DC 20005. The title *Science* is a registered trademark of AAAS.